Energy Conversion and Management 222 (2020) 113229

Contents lists available at ScienceDirect

Energy Conversion and Management

journal homepage: www.elsevier.com/locate/enconman

Dynamic modelling and analysis of an adsorption-based power and cooling cogeneration system

Yanan Zhao, Mingliang Li, Rui Long*, Zhichun Liu*, Wei Liu

School of Energy and Power Engineering, Huazhong University of Science and Technology, Wuhan 430074, PR China

ARTICLE INFO

Keywords:
Low-grade heat
Adsorption-based desalination
Reverse electrodialysis
Cogeneration
Exergy efficiency

ABSTRACT

In this study, an electricity and cooling power cogeneration system is investigated to harvest low-grade heat below 80 °C, which consists of a two-bed adsorption-based desalination (AD) system for thermally separating the salt solution into diluted and concentrated solutions while offering cooling power and a reverse electrodialysis (RED) system for converting the Gibbs free energy of mixing of the generated solutions into electricity. The dynamic response of the cogeneration system is presented first, and the asymmetric operation period is analyzed. Then the effects of adsorption/desorption time, switching time, working concentration, working fluid mass, and adsorbents on the electric efficiency, coefficient of performance (COP) and exergy efficiency of the cogeneration system are systematically evaluated. Results reveal that longer adsorption/desorption time leads to degraded electrical efficiency and exergy efficiency, and upgraded COP. Extended switching time contributes to COP and exergy efficiency, however, decreases the electric efficiency. Larger salt concentration improves the electric efficiency, however degrades the exergy efficiency and COP. Increasing working solution mass can augment the electrical efficiency, exergy efficiency and COP. Furthermore, refrigeration performance conflicts with power generation performance for different adsorbents. With CAU-10 as the adsorbent, an exergy efficiency of 30.04% is achieved, meanwhile the electric efficiency and COP is 0.39% and 0.84, respectively at adsorption/desorption time of 900 s, switching time of 10 s and working concentration of 8 mol/kg.

1. Introduction

Excessive dependence on fossil fuel combustion renders sever environmental problems, which can be alleviated by improving the energy utilization efficiency and developing new renewable and sustainable energy resources [1–3]. In the energy utilization process, 72% of the primary energy is converted into waste heat [4], and the utilization of such waste heat attracts increasing attentions [5,6]. Organic Rankine cycle (ORC) and Kalina cycle systems have been widely exploited for converting the low-grade heat into electricity [7,8]. Cataldo et al. [9] revealed an exergy efficiency of 28% when operating at the heat source temperature of 150 °C with Novec649 as the working fluid. Long et al. [10] obtained an exergy efficiency 34.41% of the Kalina cycle system 11 at the heat source temperature of 190 °C. Commercially, above thermodynamic systems are extensively employed to harvest low grade waste heat above 80 °C [8,11]. However, for temperature below 80 °C, their performance is far from satisfactory.

Recently, osmotic heat engines (OHEs) have been proposed to convert low-grade heat below 80 °C into electricity, which consist of a thermal separation module that utilizes waste heat to separate salt solutions into concentrated and diluted solutions via membrane distillation (MD) or adsorption-based desalination (AD), and a power generation module that converts the Gibbs free energy of mixing of the produced concentrated and diluted solutions into electricity by pressure retarded osmosis (PRO) or reverse electrodialysis (RED) [12–15]. In the MD process, the hydrophobic membrane allows water vapor to permeate through and prevent salt ions [16–18]. When the feed solution is heated by a low-temperature heat source, a temperature difference is established across the hydrophobic membrane, resulting in different vapor pressures on the membrane-liquid interface [19]. Driven by the transmembrane vapor pressure difference, water vapor molecules pass through the membrane and condense on the permeate stream side, generating diluted and concentrated salt solutions [20,21]. AD is considered as a promising technology that can use low temperature waste heat for fresh water and cooling cogeneration. In the AD cycle, the solvent first evaporates in the evaporator and then adsorbed by the adsorbent so that the remaining solution in the evaporator is concentrated. The solvent is then desorbed driven by an external low-grade heat source and condensed in the condenser to produce the diluted solution [22–24]. In the PRO module, driven by the

* Corresponding authors.
E-mail addresses: r_long@hust.edu.cn (R. Long), zcliu@hust.edu.cm (Z. Liu).

https://doi.org/10.1016/j.enconman.2020.113229
Received 19 May 2020; Received in revised form 13 July 2020; Accepted 14 July 2020

Nomenclature

A	Area m^2
C	Uptake of the adsorbent kg kg^{-1}
C_0	Maximum uptake of the adsorbent kg kg^{-1}
c_p	Specific heat capacity J kg^{-1} K^{-1}
D_{so}	A kinetic constant for the silica gel water system m^2 s^{-1}
E	Characteristic energy kJ mol^{-1}
E_a	Activation energy of surface diffusion kJ mol^{-1}
E_{cell}	Electromotive force of one cell V
F	Faraday constant C mol^{-1}
f	Spacer shadow factor -
h_f	Sensible heat kJ kg^{-1}
h_{fg}	Latent heat kJ kg^{-1}
I	Ion strength of a solution mol L^{-1}
J	Salt or water flux mol $s^{-1}m^{-2}$
j	Current density A m^2
L	Length of the membrane m
M	Mass kg
$\dot{m}$	Mass flow rate kg s^{-1}
n	Surface heterogeneity factor of the adsorption materials-
P	Pressure of adsorption/desorption Pa
P_s	Saturation pressure Pa
P_{RED}	Power W
Q	Heat J
$\dot{Q}$	Power W
Q_{st}	Isosteric heat of adsorption kJ kg^{-1}
R	Universal gas constant J mol^{-1} K^{-1}
R_a	Area specific resistance Ω m^2
R_p	Average radius of the adsorbent grains m
T	Temperature K
t	Time s
U	Heat transfer coefficient W m^{-2} K^{-1}
V	Volume flow rate m^3 s^{-1}
v	Specific volume m^3 kg^{-1}
W	Width of the membrane m
X	Concentration mol kg^{-1}
z	Valency of an ion -

Greek Symbols

α	Permselectivity of the ion-selective membrane in RED -
γ	Activity coefficient-
δ	Thickness m
η	Efficiency-
Λ	Molar conductivity S m^2 mol^{-1}
ρ	Density kg m^{-3}

Subscripts

abe	Adsorbate
ads	Adsorption
Brine	Concentrated brine
bed	Adsorption/desorption process
Cond	Condenser
ch	Chilled water
cw	Cooling water
d	distillate
des	desorption
diff	diffusion
Evap	Evaporator
eva	Evaporation
env	Environment
g	Gas phase
HX	Heat exchanger
HC	High concentration
hw	Hot water
in	Inlet
LC	Low concentration
m	Membrane
mig	Migration
out	Outlet
s	Salt
sb	Adsorbent
switch	Switching process
w	Cold water

Abbreviations

AD	Adsorption-based desalination
AEM	Anion exchange membrane
CEM	Cation exchange membrane
COP	Coefficient of performance
MD	Membrane distillation
OHE	Osmotic heat engines
ORC	Organic Rankine cycle
PRO	Pressure retarded osmosis
RED	Reverse electrodialysis

transmembrane osmotic pressure difference, water permeates from low concentration solution to pressurized high concentration one to offer electricity via a hydro-turbine [25]. In the RED process, ions pass through the ion exchange membranes at a salinity gradient, directly converting the Gibbs free energy of mixing into electricity via an external load [26–30].

Various kinds of OHE configurations have been developed. Olkis et al. [31] proposed a novel osmotic heat engine composed of RED and AD. 227 kinds of salts and 10 kinds of adsorption materials were investigated and an exergy efficiency up to 30% was achieved. Lin et al. [32] presented an OHE system which combines MD and PRO for heat to electricity conversion, and a theoretical energy efficiency of 9.8% was obtained with 60 and 20°C as the heat source and heat sink temperature and 1.0 M NaCl as the working solution. Long et al. [26] achieved an electrical efficiency of 1.15% with a MD-RED system when operating at 5.0 M NaCl solution. The selected salt solutions could also impact the power generation of the OHEs for different ion diffusivity and membrane selectivity. Gong et al. [33] found that $MgCl_2$ and NaCl could increase the power density, while $MgSO_4$ hinders the power extracted. Shaulsky et al. [34] evaluated the performance of the MD-PRO OHE system with LiCl-methanol as working solution and a maximum power density of 72.1 W/m^2 was achieved at a concentration of 3 M. Tamburini et al. [35] revealed that lithium ion salts show overwhelming advantages over NaCl and an exergy efficiency of 85% was achieved. Hu et al. [36] investigated an OHE composed of RED and multi-effect distillation. The energy conversion efficiency was promoted to 0.85% with the inlet hot water temperature of 95 °C and working fluid concentration of 3.5 mol/kg. Lee et al. [37] introduced an OHE which consists of PRO and multi-stage vacuum MD for converting low-grade heat into electricity and a power density of 9.7 W/m^2 was obtained. Long et al. [38] proposed an alternative kind of thermal regenerative osmotic heat engine (TROHE), which employs power-driven separation processes that run at a lower temperature, and the salinity gradient power technologies for power extraction after heating. For a TROHE that employs the reverse osmosis in the solution separation process, and pressure retarded osmosis in the energy extraction process, when operating between 60 °C and 20 °C, a maximum energy efficiency of 1.4% was achieved at 7 M LiCl-Methanol solution with a regenerative

efficiency 90%. Zhao et al. [39] proposed an alternative adsorption-based power and cooling cogeneration system, which consists of an adsorption-based desalination module and a pressure retarded osmosis module, and a maximum exergy efficiency of 33.9% was achieve at a desorption temperature of 50 ℃.

As the AD process can generate concentrated and diluted salt solutions as well as providing cooling, here we investigate an advanced osmosis heat engine that can utilize low-grade heat below 80 ℃ for electricity and cooling cogeneration, which consists of a two-bed adsorption-based desalination (AD) system for thermally separating the salt solution into diluted and concentrated solutions while offering cooling power and a reverse electrodialysis (RED) system for converting the Gibbs free energy of mixing of the generated solutions into electricity. The dynamic response of the cogeneration system is presented first, and the asymmetric operation period is analyzed. Then the effects of key parameters such as adsorption/desorption time, switching time, concentration and working fluid mass on the performance of the system are numerically evaluated in terms of some indicators such as electric efficiency, coefficient of performance (COP), and exergy efficiency. Finally, some conclusions are drawn.

2. System description and modelling

As shown in Fig. 1, the investigated electricity and cooling power cogeneration system consists of a two-bed adsorption-based desalination (AD) system for thermally separating the working salt solution into diluted and concentrated ones while offering cooling power, and a reverse electrodialysis (RED) system for converting the salinity gradient of the generated solutions into electricity. The AD system consists of an evaporator, a condenser, and a adsorption/desorption bed. Firstly, the working salt solution is fed into the evaporator. With valve 1 open and valve 2 closed, the water vapor evaporates in the evaporator and travels into the left chamber, and is absorbed by the adsorption bed while cooled by the external cooling water circuit. Meanwhile, the chilled water is cooled as the solution evaporates, offering the cooling power to the outside. At the end of the adsorption process, valve 1 and valve 2 are both closed. The cooling water circuit switches to hot water circuit to preheat the adsorbent bed, while discharging the concentrated salt solution in the evaporator. Then valve 2 is opened. The water vapor is desorbed from the bed, and is condensed in the condenser. Therefore, the diluted solution is produced. Then valve 1 and valve 2 are both closed, and the adsorbent bed is precooled for adsorption. The left and right beds operate alternately, enabling semi-continuous operation: one bed is absorbing while the other one is desorbing. In the RED module, the concentrated and diluted solutions generated from AD system are charged into RED system. Driven by salinity gradient, cation and anion diffuse from concentrated solution to diluted one through alternatively installed cation exchange membranes (CEMs) and anion exchange membranes (AEMs), forming the ionic current that is finally converted into electronic current through redox reaction on the electrodes. The power is extracted via an external load. The effluents of the RED system are mixed and recharged into the evaporator for the next cycle.

2.1. Modelling the AD system

In the AD process, kinetics and isotherm properties of the adsorbent are required to estimate the adsorbent uptake at different pressure ratios under equilibrium conditions. The adsorption isotherms can be descripted by the Dubinin–Astakhov equation [40]

$$C = C_0 \exp\left\{-\left[\frac{RT}{E}\ln\left(\frac{P_s}{P}\right)\right]^n\right\} \tag{1}$$

where C is the estimated uptake. C_0 is the maximum uptake. E is the characteristic energy. R is the universal gas constant. P is the pressure of adsorption/desorption and P_s defines the saturation pressure under the sorbent temperature T. n is a surface heterogeneity factor of the adsorption materials. The adsorption/desorption rate is given by LDF equation [41]

$$\frac{dC}{dt} = \frac{15 D_{so} e^{-\frac{Ea}{RT}}}{R_p^2}(C - C_0) \tag{2}$$

The mass balance of the system is given by

$$\frac{dM_{s,Evap}}{dt} = \dot{m}_{s,in} - \dot{m}_{d,Cond} - \dot{m}_{Brine} \tag{3}$$

here, $M_{s,Evap}$ is the amount of the working solution in the evaporator.

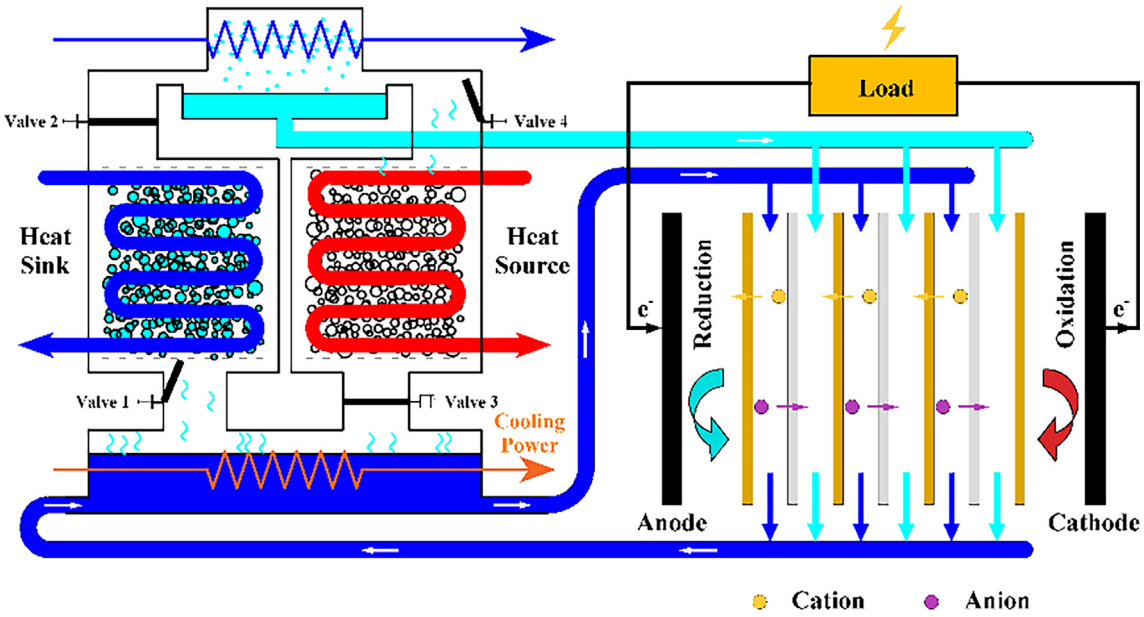

Fig. 1. Schematic diagram of the investigated electricity and cooling power cogeneration system, which consists of a two-bed adsorption-based desalination (AD) system for thermally separating the salt solution into diluted and concentrated solutions while outputting cooling power, and a reverse electrodialysis (RED) system for converting the generated salinity gradient into electricity. (For interpretation of the references to colour in this figure legend, the reader is referred to the web version of this article.)

The three items in the right hand of Eq. (3) represent mass flow rate of feed solution, diluted solution extracted from condenser and concentrated solution rejected from evaporator.

The mass and salt balance in the evaporator can be expressed as

$$\frac{dM_{s,Evap}}{dt} = \dot{m}_{s,in} - \dot{m}_{Brine} - \left(\frac{dC_{ads}}{dt}\right)M_{sb} \tag{4}$$

$$M_{s,Evap}\frac{dX_{s,Evap}}{dt} = X_{s,in}\dot{m}_{s,in} - X_{s,Evap}\dot{m}_{Brine} - X_D\left(\frac{dC_{ads}}{dt}\right)M_{sb} \tag{5}$$

where $X_{s,in}$ and $X_{s,Evap}$ are the working concentration and real-time solution in the evaporator, X_D is the vapor concentration, M_{sb} is the mass of the adsorbent.

In the evaporator, the solution evaporates and absorbs the heat from the refrigerant. Therefore, the refrigerant is chilled. The energy balance can be written as

$$\begin{aligned}&[M_{s,Evap}c_{p,s}(T_{Evap}, X_{s,Evap}) + M_{HX,Evap}c_{p,HX}]\frac{dT_{Evap}}{dt}\\ &= h_f(T_{Evap}, X_{s,Evap})\dot{m}_{s,in} - h_{fg}(T_{Evap})\frac{dC_{ads}}{dt}M_{sb} + \dot{m}_{ch}c_{p,ch}\\ &\quad (T_{ch,in} - T_{ch,out}) - h_f(T_{Evap}, X_{s,Evap})\dot{m}_{Brine}\end{aligned} \tag{6}$$

where $M_{HX,Evap}$ is the mass of the heat exchanger in the evaporator. The terms in the right hand of Eq. (6) denotes the sensible heat of the feed solution, latent heat taken away by the adsorbed vapor, heat adsorbed from the refrigerant and the sensible heat removal through the discharged brine, respectively. h_f and c_p represent latent heat and specific heat both as functions of temperature and concentration, h_{fg} denotes the latent heat of gaseous phase as a function of temperature. And the temperatures of the outlet water from each heat exchangers can be calculated as

$$T_{out} = T_0 + (T_{in} - T_0)\exp\left(\frac{-UA}{\dot{m}c_p(T_0)}\right) \tag{7}$$

here, T_0 and A is the temperature and area of the heat exchanger.

In the condenser, the adsorbed vapor is condensed by the cold water. The energy balance is written as

$$\begin{aligned}&[M_{Cond}c_p(T_{Cond}) + M_{HX,Cond}c_{p,HX}]\frac{dT_{Cond}}{dt} = h_f(T_{Cond})\frac{dM_d}{dt}\\ &\quad + h_{fg}(T_{Cond})\frac{dC_{des}}{dt}M_{sb} + \dot{m}_w c_{p,w}(T_{w,in} - T_{w,out})\end{aligned} \tag{8}$$

where M_d is the mass of the diluted solution. M_{Cond} is the mass of the condensed solution. C_{des} denotes the desorbed water vapor uptake and $\dot{m}_w$ is the mass flow rate of the cold water in the condenser.

The energy balance in adsorption/desorption bed which consists of adsorbent, adsorbate and heat exchanger with cooling/hot water external circuit can be given by

$$\begin{aligned}&[M_{sb}c_{p,sb} + M_{HX}c_{p,HX} + M_{abe}c_{p,a}]\frac{dT_{ads/des}}{dt} = \pm Q_{st}M_{sb}\frac{dC_{ads/des}}{dt}\\ &\quad \pm \dot{m}_{cw/hw}c_p(T_{cw/hw})(T_{cw/hw,in} - T_{cw/hw,out})\end{aligned} \tag{9}$$

where M_{abe} is the mass of the absorbed vapor. $T_{cw/hw}$ denotes the temperature of the cooling water/hot water and Q_{st} is the isosteric heat of adsorption which can be calculated as [42]

$$Q_{st} = h_{fg} + E\left\{-\ln\left(\frac{C}{C_0}\right)^{1/n}\right\} + Tv_g\left(\frac{\partial P}{\partial T}\right)_g \tag{10}$$

where v_g represent the volume of gaseous phase.

The heat required for the entire cycle can be calculated by

$$Q_{des} = \int_0^{t_{cycle}} \dot{m}_{hw}c_{p,hw}(T_{hw,in} - T_{hw,out})dt \tag{11}$$

where the cycle time is composed of adsorption/desorption time and switching time, that is $t_{cycle} = t_{bed} + t_{switch}$, and the heat consumption rate can be calculated as $\dot{Q}_{des} = Q_{des}/t_{cycle}$.

The outputting cooling power can be calculated by

$$\dot{Q}_c = \frac{1}{t_{cycle}}\int_0^{t_{cycle}} \dot{m}_{ch}c_{p,cw}(T_{ch,in} - T_{ch,out})dt \tag{12}$$

2.2. Modelling the RED system

In the RED process, the concentrated and diluted solutions produced in AD system enter into RED, and NaCl solution is selected as the working solution in this study. The voltage of RED caused by the Nernst potential difference between the CEM and the AEM can be calculated as [43]

$$E_{cell}(x) = \alpha_{CEM}\frac{RT}{F}\ln\frac{\gamma_{HC}^{Na}(x)X_{HC}(x)}{\gamma_{LC}^{Na}(x)X_{LC}(x)} + \alpha_{AEM}\frac{RT}{F}\ln\frac{\gamma_{HC}^{Cl}(x)X_{HC}(x)}{\gamma_{LC}^{Cl}(x)X_{LC}(x)} \tag{13}$$

where α is the permselectivity of the ion-selective membrane, F is the Faraday constant, X denotes the concentration and the subscripts HC and LC represent high and low concentration, respectively. γ is the activity coefficient which is given by Debye-Huckel equation [44]

$$\gamma(x) = \exp\left[\frac{-0.51z^2\sqrt{I(x)}}{1 + (A/305)\sqrt{I(x)}}\right] \tag{14}$$

where I is the ion strength, A denotes the effective hydrated ion radius and z is the valency of the ion.

Considering the RED resistance, the area specific resistance of the cell can be calculated as [43–45]

$$R_{a,cell} = R_{LC}(x) + R_{HC}(x) + R_{AEM} + R_{CEM} \tag{15}$$

where $R_{LC} = f\frac{\delta_{LC}}{\Lambda_{LC}X_{LC}(x)}$ and $R_{HC} = f\frac{\delta_{HC}}{\Lambda_{HC}X_{HC}(x)}$, Λ refers to is the molar conductivity, δ_{LC} and δ_{HC} are the thicknesses of LC and HC compartment, f is an spacer shadow factor. R_{AEM} and R_{CEM} are the area resistance of cation exchange membrane and anion exchange membrane.

According to the Ohm's law, the space-dependent current density can be developed as

$$j(x) = \frac{E_{cell}(x)}{R_{a,cell}(x) + R_{a,ext}(x)} \tag{16}$$

where $R_{a,ext}(x)$ is the resistance of the external load.

The salt flux through the membrane contains two parts, one is migration term, which is responsible for generating current, and the other is diffusion term, which is detrimental [44,46]

$$J_{total}(x) = J_{mig}(x) + J_{diff}(x) = \frac{j(x)}{F} + \frac{2D_{salt}}{\delta_m}[X_{HC}(x) - X_{LC}(x)] \tag{17}$$

where D is the salt permeability coefficient.

In addition, there is also a water flux from the LC to the HC solution cell due to the osmosis [47]

$$J_{water}(x) = -\frac{2D_{water}}{\delta_m}[X_{HC}(x) - X_{LC}(x)]\frac{M_{H_2O}}{\rho_{H_2O}} \tag{18}$$

The mass balance equations are finally developed as [44]

$$\frac{dX_{HC}(x)}{dx} = -\frac{W}{V_{HC}}J_{total}(x) - X_{HC}(x)\frac{WJ_{water}(x)}{V_{HC}} \tag{19}$$

$$\frac{dX_{LC}(x)}{dx} = \frac{W}{V_{LC}}J_{total}(x) + X_{LC}(x)\frac{WJ_{water}(x)}{V_{LC}} \tag{20}$$

where V is the volume flow rate and W is the width of the membrane.

When the external load is equal to the internal resistance, the maximum of power can be obtained $P_{d,max}(x) = \frac{1}{2}j(x)^2R_{a,cell}(x)$, so that the total power can be calculated as

$$P_{RED} = W\int_0^L P_{d,max}(x)dx \tag{21}$$

where L is the length of the membrane.

2.3. Overall performance of the cogeneration system

To characterizing the overall performance of the cogeneration system, some indicators are employed. For electricity supply, the electric efficiency is calculated as $\eta_e = W_{RED}/Q_{des}$. As a refrigerator, the refrigeration performance of the system is evaluated by the coefficient of performance $COP = Q_c/Q_{des}$. Considering the difference between cooling power and electricity in energy quality, exergy efficiency is employed to evaluate the overall performance of the hybrid cogeneration system

$$\eta_{ex} = \frac{Q_c\left(\frac{T_{env}}{T_{eva}} - 1\right) + W_{RED}}{Q_{des}\left(1 - \frac{T_{env}}{T_{des}}\right)} \quad (22)$$

where T_{env} is the environmental temperature, W_{RED} is the work extract in a cycle.

3. Results and discussion

3.1. Model validation

Alsaman et al. [48] proposed a adsorption desalination-cooling system to harvest solar energy. The effects of cycle time and hot water/cold water inlet temperature on the performance of the system in terms of specific daily water production (SDWP), specific cooling power (SCP) and COP were studied experimentally. Validation of the AD model we investigated is based on the comparison of SDWP and the specific cooling power SCP between the present calculation and the experiment data of Alsaman et al. [48] with hot water inlet temperature ranging from 76.2 to 92.5 ℃. As shown in Fig. 2, a good accordance exists between the calculated data and the experimental one, which validates the dynamic model employed in present study. The AD model in Alsaman's research is for sea water desalination. In present cogeneration system, which consists of a two-bed AD system for thermally separating the salt solution into diluted and concentrated solutions while offering cooling power and a RED system for power generation, NaCl aqueous solution is employed as the working solution. We have revised the solution-depended parameters in the model for our study, such as the concentration depended evaporation pressure via coupling the osmotic coefficient of the salt solution.

3.2. Dynamic response of hybrid cogeneration system

We first analyze the dynamic characteristics of the cogeneration system. The inlet temperatures of hot and cooled water for the desorption/adsorption bed are 343.15 K and 293.15 K, respectively. The inlet temperatures of the chilled water and cold water in the evaporator and condenser are both fixed at 293.15 K. The environmental temperature is set at 293.15 K. Silica gel is employed as the adsorbent, and the mass of adsorbent is 6.75 kg. The number of RED cells is 1000. The adsorption/desorption time of the physical bed t_{bed} is 900 s and the switching time t_{switch} is 10 s. The mathematical model of the adsorption-based cogeneration system is solved via the MATLAB platform and it reaches the steady-state cycle condition in 4–5 cycles after the beginning of the computation. Fig. 3 shows the temperature–time histories of the bed 1, bed 2, evaporator and condenser of the AD system. The system consists of two physical beds for semi-continuous operation where one bed is adsorbing while the other is desorbing, resulting in a periodical temperature variation of the adsorption bed. Each bed goes through four processes asynchronously: Firstly, pre-heat the bed to prepare for the desorption; Then heat up the adsorption bed while desorbing; After the desorption process, pre-cool the bed for the adsorption; Finally cool the bed until the end of adsorption process. The temperature in the evaporator is lower than the ambient temperature in the evaporation process. The chilled refrigerant provides cooling power to the outside.

As shown in Fig. 4a, the water production displays periodic variation. In a cycle, there is always a bed in desorption state. The water production increases during t_{bed}, and at the end of the desorption process, the water production reaches the peak value. During the switch time, the water production becomes zero, which is caused by closing valves connecting to evaporator and condenser during switching time. Due to water evaporation, the mass of solvent in the evaporator decreases, resulting in concentrated solution in the evaporator, as shown in Fig. 4b. The variation of the salt concentration in the evaporator C_{eva} and water production exhibit the same behavior. The concentrated and diluted solution are discharged during the switch time, which are feed into RED system for generating electricity.

To guarantee a stable operation, the produced concentrated and diluted solutions are stored and then fed into the RED system with time averaged volume flow rate. The operation period of RED should not be larger than that of AD cycle, and different t_{RED} corresponds to varying flow rate of working fluid that determines the electric power. Here, the performance of the system under different t_{RED}/t_{AD} is investigated. Fig. 5a shows the electric power of RED under different t_{RED}/t_{AD}, the area surrounded by the power curve and horizontal ordinate represents the work extracted in a cycle. The reduction of t_{RED} leads to increased volume flow rates of the working solution feed into RED system, resulting in augmented real-time power P_{RED}. We can obtain a larger intermittent output power by adjusting the operating time of RED to meet some special application. As seen in Fig. 5b, the electric efficiency increases with increasing t_{RED}/t_{AD}. Since the cooling performance of the AD process is independent of t_{RED}, the exergy efficiency increases for augmented electrical efficiency. When t_{RED} is equal to t_{AD}, the maximum work can be extracted for decreased pump loss and electric resistance dissipation. Therefore, in the following discussions we only focus on the situation where $t_{RED} = t_{AD}$.

3.3. The effect of adsorption/desorption time

Adsorption/desorption time t_{bed} refers to the duration when the physical bed is in the process of adsorption or desorption and is connected to either the evaporator or the condenser, thus to generate concentrated and diluted solutions. Here the effect of t_{bed} on the performance of the system are investigated. The switching time is set at 20 s and the working concentration is 8 mol/kg. As shown in Fig. 6a, with the increasing t_{bed}, the desorption heat power and cooling power both decrease. It could be attributed to that at the beginning of t_{bed}, due to the larger heat transfer temperature difference, the heat transfer rate

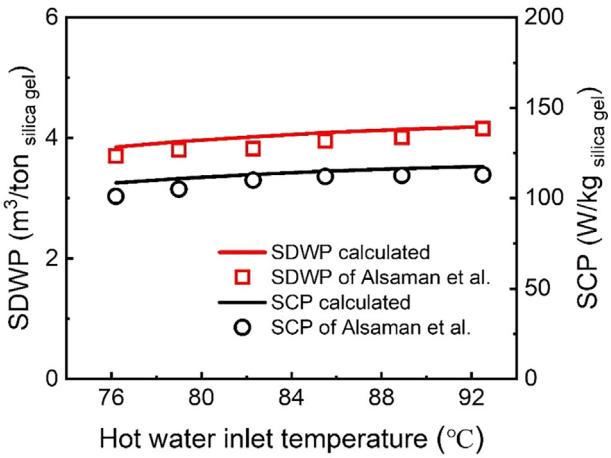

Fig. 2. Comparison of the specific daily water production (SDWP) and the specific cooling power (SCP) between present calculation and that of Alsaman et al. with hot water inlet temperature ranging from 76.2 to 92.5 ℃ and silica gel as the adsorbent.

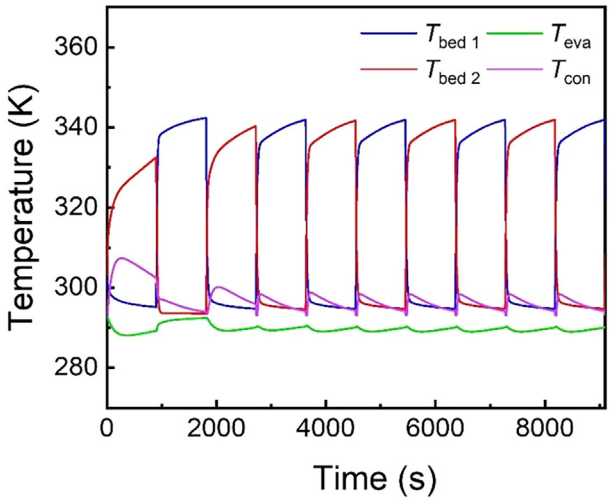

Fig. 3. Temperature-time histories of the adsorption bed, desorption bed, evaporator and condenser of the absorption-based desalination system.

is higher than that at the end, which leads to a reduced desorption heat power with the extension of adsorption/desorption time. Larger adsorption/desorption time indicates the adsorbent contacts with the water vapor in a longer time, which is benefit for adsorption/desorption, leading to increased working capacity, as shown in Fig. 6b. Work capacity represents the mass of water vaper adsorbed per kilogram of adsorbent, so it shows the same trend as the water production for specified adsorbent. With the increase of t_{bed}, the water production and the concentration of the concentrated solution increase accordingly, contributing to the work extracted in RED. As the increase of the work extracted is less than that of the cycle period, resulting in the reduced power output. With the increase of adsorption/desorption time, the reduction of the $\dot{Q}_{des}$ is much obvious than that of cooling power but less than that of P_{RED}. Therefore, as depicted in Fig. 7, the COP increase with increasing t_{bed} while the electric efficiency and the exergy efficiency decrease with increasing t_{bed}.

3.4. The effect of switching time

Switching time t_{switch} refers to the time when the physical bed is in the process of preheating/precooling and is not connected to neither the condenser nor the evaporator. During the switching time, the desorption bed is preheated to raise the bed pressure until the pressure is equal to the pressure in the condenser and the adsorption bed is precooled to reduce the temperature and pressure of the bed until the pressure matches up the pressure in the evaporator. For unmatched longer switching time, the water production of each cycle increases with the increase of the switching time. However increasing switching time increases the cycle period, which decreases the power output. For unmatched shorter switching time, the adsorption bed is first subjected to pressure swing desorption. The vapor may condense in the evaporator before starting the actual adsorption process. In the condensing process, the desorption bed may adsorb vapor from the condenser. Here a switch time of 10 ~ 40 s is selected by referencing previous researches on adsorption desalination [49,50]. As shown in Fig. 8, without the enough switching time to precool the adsorption bed, the water production is deteriorated due to the poor work capacity. And the cooling power will be reduced simultaneously. $\dot{Q}_{des}$ decreases with the extension of the switching time since the adsorption bed is in the preheated process with low heat consumption. During switching time, the evaporation is stopped so that cooling power and P_{RED} are both reduced. As shown in Fig. 8a, the reduction of $\dot{Q}_{des}$ with switch time is less than that of P_{RED}, resulting in decreased η_e. As the cooling power is obviously lager than P_{RED} and longer t_{switch} significantly elevates COP. The exergy efficiency increases with increasing switching time, as depicted in Fig. 9.

3.5. The effect of working concentration

Fig. 10 shows the effect of working concentration on the performance of the system. Higher working concentration lowers the evaporation pressure and thus the working capacity of the physical bed. As the concentration increases, the adsorption process is weakened, resulting in poorer cooling performance and decreased water production. Therefore, the cooling power and $\dot{Q}_{des}$ decreases as depicted in Fig. 10a. Although higher working concentration reduces the water production and the volume flow rate of generated concentrated and diluted solutions fed into the RED system, the impact of the improved transmembrane salinity gradient in RED is more dominant, leading to an augmented P_{RED}. As shown in Fig. 11, $\dot{Q}_{des}$ and cooling power both decrease with the increase of working concentration. As the decrease of $\dot{Q}_{des}$ overrides the impact of cooling power, COP decrease. η_e increases with increasing working concentration for upgraded P_{RED}. The impact of cooling reduction exceeds the power increase, resulting in the degraded exergy efficiency.

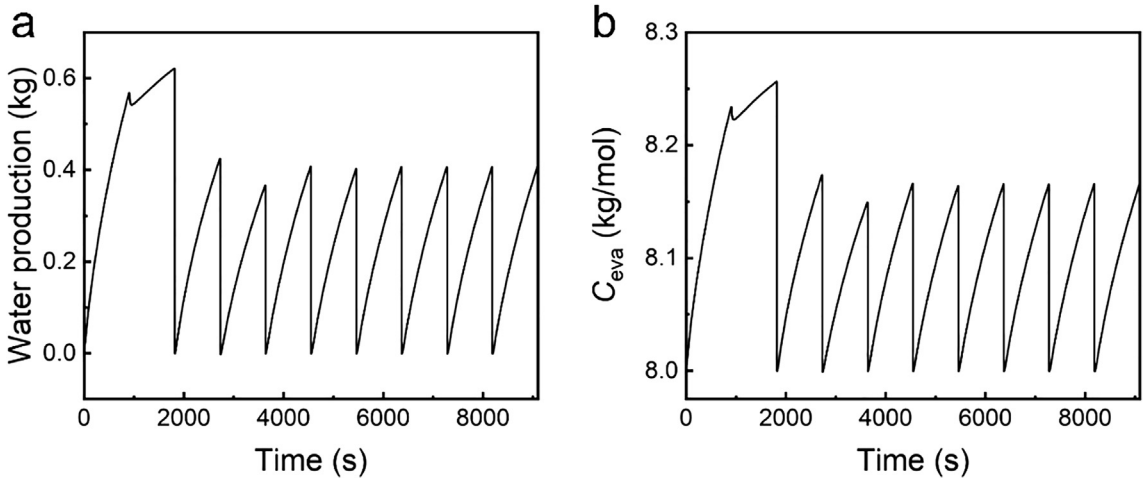

Fig. 4. Temporal history of the water production (a) and the concentration of the solution in the evaporator (b). In this case, the cycle time of AD is equal to that of RED.

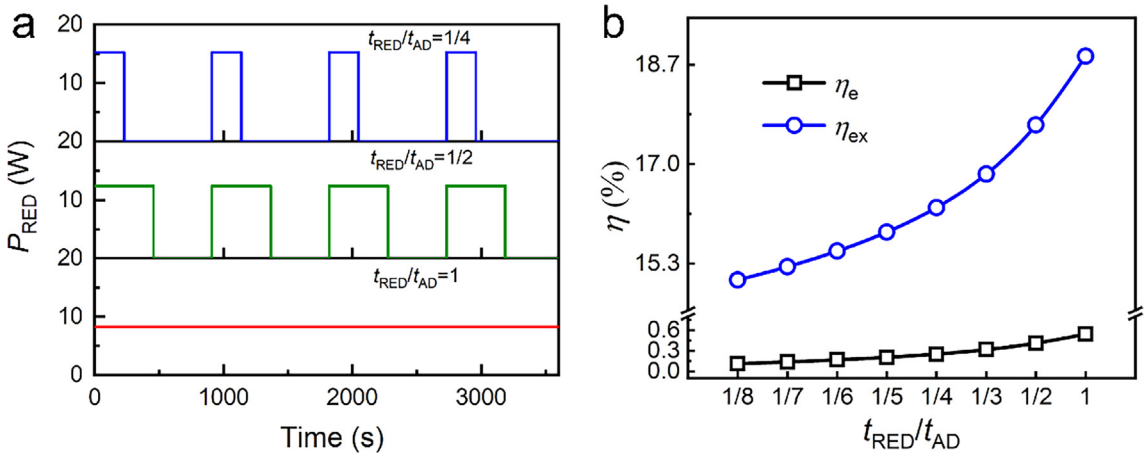

Fig. 5. Electric power of RED (a), electric efficiency and exergy efficiency (b) under different t_{RED}/t_{AD} at t_{bed} of 900 s, t_{switch} of 10 s and working concentration of 8 mol/kg. (For interpretation of the references to colour in this figure legend, the reader is referred to the web version of this article.)

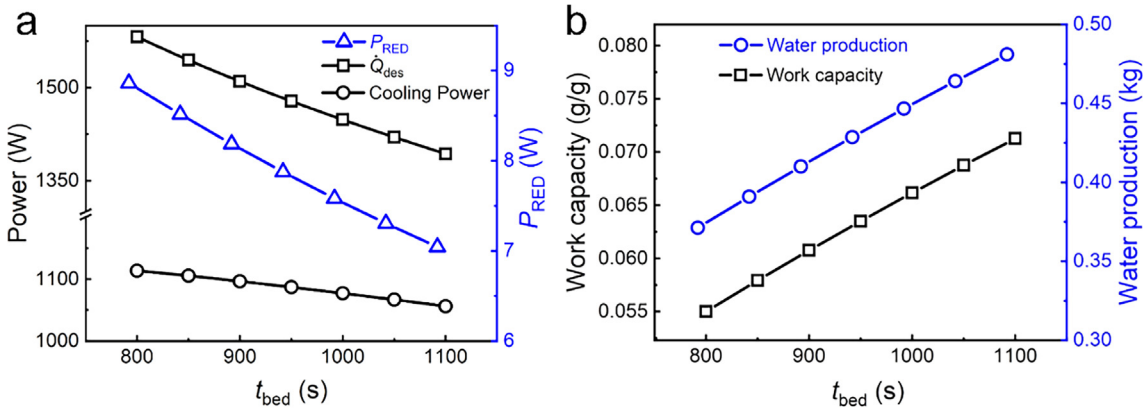

Fig. 6. Desorption heat power, cooling power and electric power (a), Work capacity of the adsorbent and water production (b) in a cycle under different adsorption/desorption time.

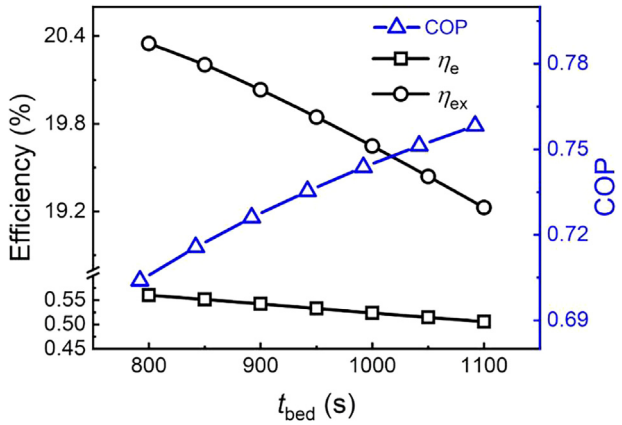

Fig. 7. Electric efficiency, COP and exergy efficiency of the investigated adsorption-based power and cooling cogeneration system under different adsorption/desorption time.

3.6. The effect of working fluid mass

The adsorption-based cogeneration system is a closed-loop system. The working fluid is first fed in the evaporator and is thermally separated into a diluted solution and a concentrated solution for power generation in the RED module. Therefore, the effect of working fluid mass on the system performance is assignable. As depicted in Fig. 12, with the increase of the working fluid mass, the work capacity increases due to deduced evaporation pressure variation, indicating that the evaporation and adsorption processes are enhanced. Therefore, the solvent evaporated in the evaporator increases, absorbing more heat from the chilled water. Thereby the cooling power is increased. The volume flow rate of diluted and concentrated solutions into RED are also increased, leading to upgraded P_{RED}. As shown in Fig. 13, COP, η_e and exergy efficiency all increase with the increasing working fluid mass, due to much significant increase of cooling power and P_{RED} than that of $\dot{Q}_{des}$.

3.7. Performance under different adsorbents

The performance of the investigated adsorption-based power and cooling cogeneration system under different adsorbents is depicted in Fig. 14. The adsorption/desorption time is set at 1000 s and the switching time is set at 10 s for 8 mol/kg NaCl solution. Since the thermal separation of salt solutions occurs in the adsorption-based desalination system, the properties of adsorbents determine the work capacity, which significantly impacts the performance of the cogeneration system. As shown in Fig. 14, the refrigeration performance conflicts with the power generation performance for various adsorbents. CAU-10 leads to the largest COP, however induces the least electric efficiency. MIL-101 results in the lowest COP while the highest electric efficiency. The exergy efficiency under different adsorbents presents the same trend with the COP as the cooling power is much larger than the electric power. CAU-10 shows an overall advantage over the other three adsorbents with an exergy efficiency of 30.04%, while MIL-101rendes the lowest exergy efficiency of 11.84%.

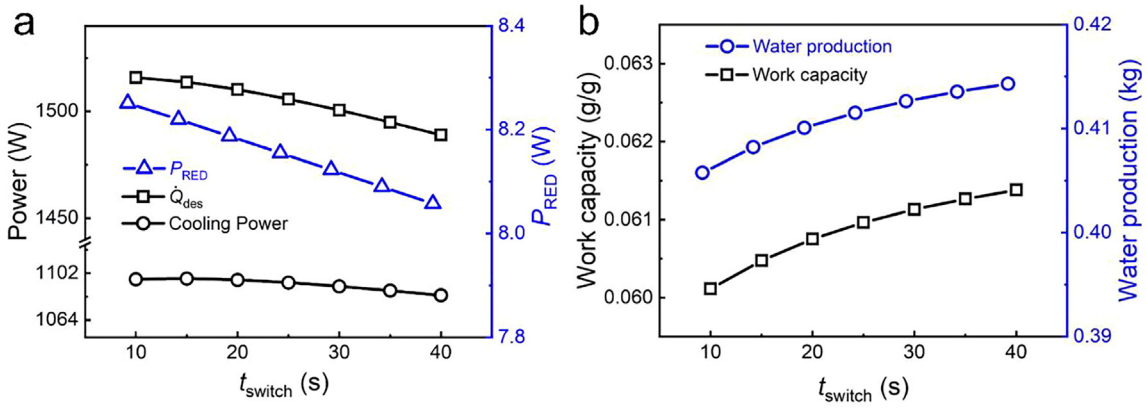

Fig. 8. Desorption heat power, cooling power and electric power (a), Work capacity of the adsorbent and water production (b) in a cycle under different switching time.

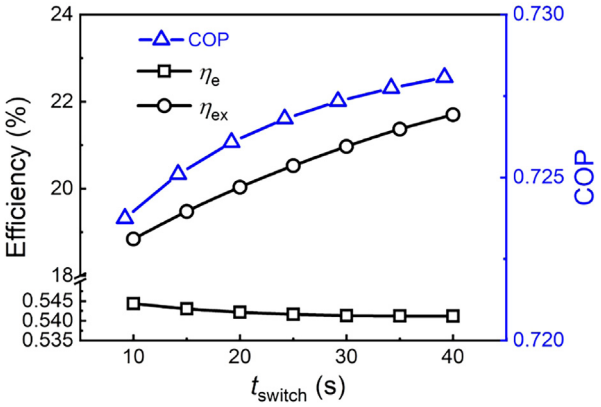

Fig. 9. Electric efficiency, COP and exergy efficiency of the investigated adsorption-based power and cooling cogeneration system under different switching time.

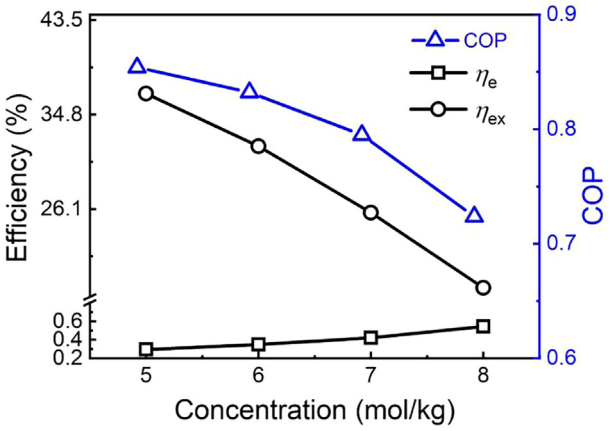

Fig. 11. Electric efficiency, COP and exergy efficiency of the investigated adsorption-based power and cooling cogeneration system under different concentration of solution.

4. Conclusions

In this study, we investigate an advanced osmosis heat engine that can utilize low-grade heat below 80 ℃ for power and cooling cogeneration, which consists of a two-bed adsorption-based desalination (AD) system for thermally separating the salt solution into diluted and concentrated solutions while offering cooling power and a reverse electrodialysis (RED) system for converting the Gibbs free energy of mixing of the generated solutions into electricity. The dynamic response of the cogeneration system is presented first, and the asymmetric operation period is analyzed. When the operation period of RED is equal to that of AD cycle, the hybrid system achieves its maximum exergy efficiency. Then the effects of adsorption/desorption time, switching time, working concentration, working fluid mass, and adsorbents on the electric efficiency, coefficient of performance (COP) and exergy efficiency of the cogeneration system are evaluated. Results reveal that to improve the cooling performance, we can extend the adsorption time and switching time, reduce the concentration and increase the mass of the working solution. If the power generation should be addressed, we

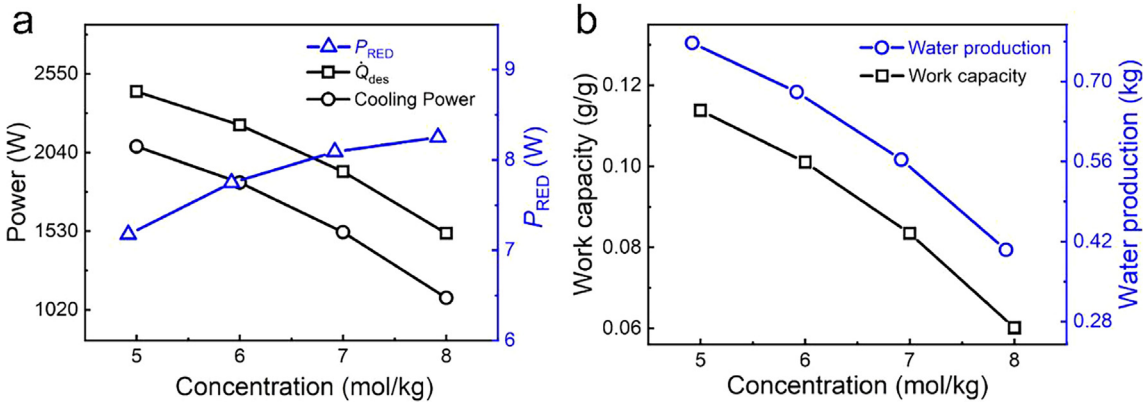

Fig. 10. Desorption heat power, cooling power and electric power (a), Work capacity of the adsorbent and water production (b) in a cycle under different concentration of solution at t_{bed} of 900 s and t_{switch} of 10 s.

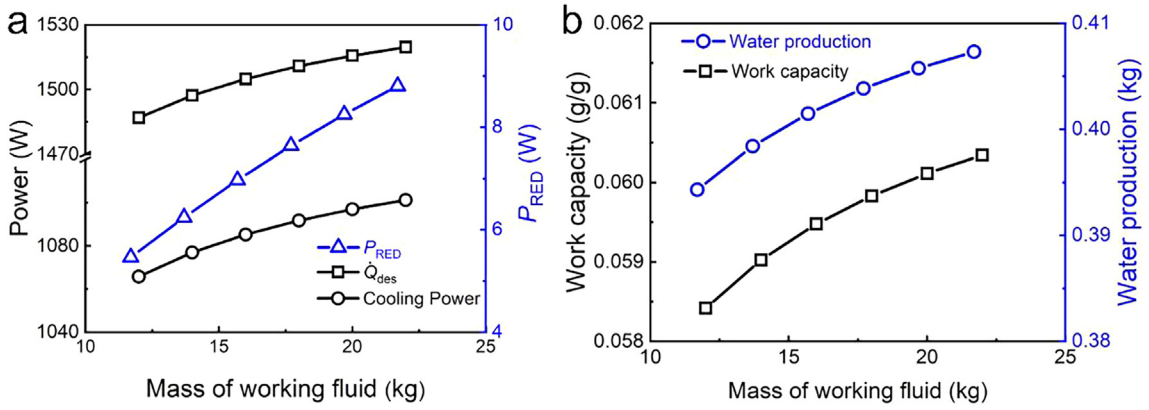

Fig. 12. Desorption heat power, cooling power and electric power (a), Work capacity of the adsorbent and water production (b) in a cycle under different mass of working fluid at t_{bed} of 900 s, t_{switch} of 10 s and working concentration of 8 mol/kg.

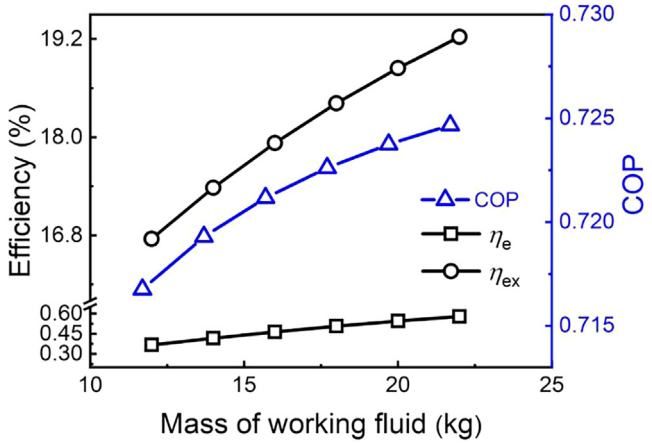

Fig. 13. Electric efficiency, COP and exergy efficiency of the investigated adsorption-based power and cooling cogeneration system under different mass of working fluid.

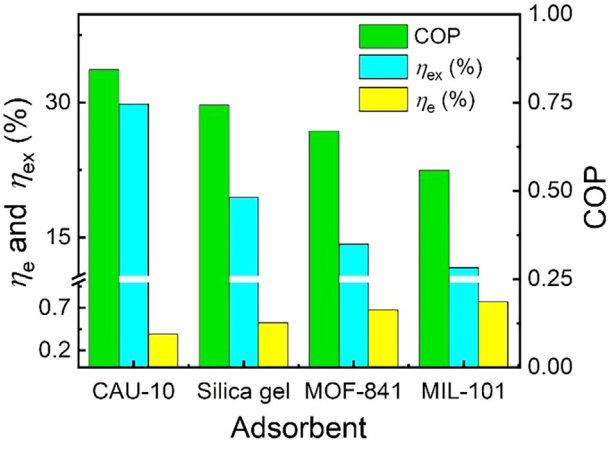

Fig. 14. COP, η_e and η_{ex} of the investigated adsorption-based power and cooling cogeneration system under different adsorbents.

can shorten the adsorption time, shorten the switching time, increase the concentration and mass of the working solution. If we focus on the overall energy utilization degree, to improve the exergy efficiency, we can shorten the adsorption time, extend the switching time, reduce the concentration and increase the mass of the working solution. By comparing the effects of different adsorbents on the system performance, we can intuitively observe the trade-off between refrigeration and power generation in the system, and CAU-10 presents advantages in exergy efficiency among the four selected adsorbents. With CAU-10 as the adsorbent, an exergy efficiency of 30.04% is achieved, meanwhile the electric efficiency and COP is 0.39% and 0.84, respectively at adsorption/desorption time of 900 s, switching time of 10 s and working concentration of 8 mol/kg.

CRediT authorship contribution statement

Yanan Zhao: Writing - original draft, Visualization. **Mingliang Li:** Formal analysis. **Rui Long:** Methodology, Writing - review & editing, Funding acquisition. **Zhichun Liu:** Conceptualization. **Wei Liu:** Formal analysis, Funding acquisition.

Declaration of Competing Interest

The authors declare that they have no known competing financial interests or personal relationships that could have appeared to influence the work reported in this paper.

Acknowledgements

This work was financially supported by the National Natural Science Foundation of China (51706076, 51736004).

References

[1] Chu S, Majumdar AJN. Opportunities and challenges for a sustainable energy future. Nature 2012;488(7411):294–303.
[2] Krajačić G, Vujanović M, Duić N, Kılkış Ş, Rosen MA, Ahmad Al-Nimr Md. Integrated approach for sustainable development of energy, water and environment systems. Energy Convers Manage 2018;159:398–412.
[3] Long R, Li B, Liu Z, Liu W. Performance analysis of a solar-powered electrochemical refrigerator. Chem Eng J.
[4] Forman C, Muritala IK, Pardemann R, Meyer BJR, Reviews SE. Estimating the global waste heat potential. Renew Sustain Energy Rev 2016;57:1568–79.
[5] Xi L, Cao X, Mo Y, Kang X, Zhang X, Peng L, et al. Power generation by coupling reverse electrodialysis and ammonium bicarbonate: Implication for recovery of waste heat. Electrochem Commun 2012;19:25–8.
[6] Long R, Li B, Liu Z, Liu W. Performance analysis of a dual loop thermally regenerative electrochemical cycle for waste heat recovery. Energy 2016;107:388–95.
[7] Kim DK, Choi HW, Kim MS. Design of a rotary expander as an expansion device integrated into organic Rankine cycle (ORC) to recover low-grade waste heat. Appl Therm Eng 2019;163:114326.
[8] Nuwayhid RY, Shihadeh A. Ghaddar NJEc, management. Development and testing of a domestic woodstove thermoelectric generator with natural convection cooling. Energy Convers Manage 2005;46(9–10):1631–43.
[9] Cataldo F, Mastrullo R, Mauro AW, Vanoli GPJE. Fluid selection of Organic Rankine Cycle for low-temperature waste heat recovery based on thermal optimization. Energy. 2014;72:159–67.
[10] Long R, Kuang Z, Li B, Liu Z, Liu WJEP. Exergy analysis and performance optimization of Kalina cycle system 11 (KCS-11) for low grade waste heat recovery. Energy Procedia 2019;158:1354–9.

[11] Schuster A, Karellas S. Kakaras E, Spliethoff HJAte. Energetic and economic investigation of Organic Rankine Cycle applications. Appl Therm Eng 2009;29(8–9):1809–17.
[12] McCutcheon JR, McGinnis RL, Elimelech M. Desalination by ammonia–carbon dioxide forward osmosis: Influence of draw and feed solution concentrations on process performance. J Membr Sci 2006;278(1):114–23.
[13] Jellinek HH. Osmosis process for producing energy. Google Patents; 1976.
[14] McGinnis RL, McCutcheon JR, Elimelech M. A novel ammonia–carbon dioxide osmotic heat engine for power generation. J Membr Sci 2007;305(1–2):13–9.
[15] Hickenbottom KL, Vanneste J, Miller-Robbie L, Deshmukh A, Elimelech M, Heeley MB, et al. Techno-economic assessment of a closed-loop osmotic heat engine. J Membrane Sci. 2017;535:178–87.
[16] Lin S, Yip NY, Elimelech M. Direct contact membrane distillation with heat recovery: Thermodynamic insights from module scale modeling. J Membr Sci 2014;453:498–515.
[17] Alkhudhiri A, Darwish N, Hilal N. Membrane distillation: A comprehensive review. Desalination 2012;287:2–18.
[18] Miladi R, Frikha N, Kheiri A, Gabsi S. Energetic performance analysis of seawater desalination with a solar membrane distillation. Energy Convers Manage 2019;185:143–54.
[19] Kuang Z, Long R, Liu Z, Liu W. Analysis of temperature and concentration polarizations for performance improvement in direct contact membrane distillation. Int J Heat Mass Tran. 2019;145:118724.
[20] Long R, Lai X, Liu Z, Liu W. Direct contact membrane distillation system for waste heat recovery: Modelling and multi-objective optimization. Energy. 2018;148:1060–8.
[21] Elzahaby AM, Kabeel AE, Bassuoni MM, Elbar ARA. Direct contact membrane water distillation assisted with solar energy. Energy Convers Manage 2016;110:397–406.
[22] Wu JW, Biggs MJ, Hu EJ. Thermodynamic analysis of an adsorption-based desalination cycle. Chem Eng Res Des 2010;88(12):1541–7.
[23] Naeimi A, Nowee SM, Akhlaghi Amiri HA. Numerical simulation and theoretical investigation of a multi-cycle dual-evaporator adsorption desalination and cooling system. Chem Eng Res Des 2020;156:402–13.
[24] Dakkama HJ, Youssef PG, Al-Dadah RK, Mahmoud S. Adsorption ice making and water desalination system using metal organic frameworks/water pair. Energy Convers Manage 2017;142:53–61.
[25] Benjamin J, Arias ME, Zhang QJD. A techno-economic process model for pressure retarded osmosis based energy recovery in desalination plants. Desalination 2020;476:114218.
[26] Long R, Li B, Liu Z, Liu W. Hybrid membrane distillation-reverse electrodialysis electricity generation system to harvest low-grade thermal energy. J Membr Sci 2017;525:107–15.
[27] Giacalone F, Papapetrou M, Kosmadakis G, Tamburini A, Micale G, Cipollina A. Application of reverse electrodialysis to site-specific types of saline solutions: A techno-economic assessment. Energy 2019;181:532–47.
[28] Giacalone F, Catrini P, Tamburini A, Cipollina A, Piacentino A, Micale G. Exergy analysis of reverse electrodialysis. Energ Convers Manage. 2018;164:588–602.
[29] Long R, Kuang Z, Liu Z, Liu W. Ionic thermal up-diffusion in nanofluidic salinity gradient energy harvesting. Natl Sci Rev 2019;6(6):1266–73.
[30] Long R, Luo Z, Kuang Z, Liu Z, Liu W. Effects of heat transfer and the membrane thermal conductivity on the thermally nanofluidic salinity gradient energy conversion. Nano Energy 2019;104284.
[31] Olkis C, Santori G, Brandani SJAE. An adsorption reverse electrodialysis system for the generation of electricity from low-grade heat. Appl Energy 2018;231:222–34.
[32] Lin S, Yip NY, Cath TY, Osuji CO. Elimelech MJEs, technology. Hybrid pressure retarded osmosis–membrane distillation system for power generation from low-grade heat: thermodynamic analysis and energy efficiency. Environ Sci Technol 2014;48(9):5306–13.
[33] Gong H, Anastasio DD, Wang K, McCutcheon JR. Finding better draw solutes for osmotic heat engines: Understanding transport of ions during pressure retarded osmosis. Desalination 2017;421:32–9.
[34] Shaulsky E, Boo C, Lin S, Elimelech M. Membrane-based osmotic heat engine with organic solvent for enhanced power generation from low-grade heat. Environ Sci Technol 2015;49(9):5820–7.
[35] Tamburini A, Tedesco M, Cipollina A, Micale G, Ciofalo M, Papapetrou M, et al. Reverse electrodialysis heat engine for sustainable power production. Appl Energy 2017;206:1334–53.
[36] Hu J, Xu S, Wu X, Wu D, Jin D, Wang P, et al. Theoretical simulation and evaluation for the performance of the hybrid multi-effect distillation—reverse electrodialysis power generation system. Desalination 2018;443:172–83.
[37] Lee J-G, Kim Y-D, Shim S-M, Im B-G, Kim W-S. Numerical study of a hybrid multi-stage vacuum membrane distillation and pressure-retarded osmosis system. Desalination 2015;363:82–91.
[38] Long R, Zhao Y, Luo Z, Li L, Liu Z, Liu W. Alternative thermal regenerative osmotic heat engines for low-grade heat harvesting. Energy. 2020;195:117042.
[39] Zhao Y, Luo Z, Long R, Liu Z, Liu W. Performance evaluations of an adsorption-based power and cooling cogeneration system under different operative conditions and working fluids. Energy 2020;204:117993.
[40] Askalany AA, Salem M, Ismail IM, Ali AHH, Morsy MG. Experimental study on adsorption–desorption characteristics of granular activated carbon/R134a pair. Int J Refrig 2012;35(3):494–8.
[41] Saha BB, Kashiwagi TJAT. Experimental investigation of an advanced adsorption refrigeration cycle. ASHRAE Trans 1997;103:50.
[42] Ruthven DM. Fundamentals of adsorption equilibrium and kinetics in microporous solids. Adsorption and Diffusion. Springer; 2006. p. 1–43.
[43] Veerman J, Post J, Saakes M, Metz S, Harmsen G. Reducing power losses caused by ionic shortcut currents in reverse electrodialysis stacks by a validated model. J Membr Sci 2008;310(1–2):418–30.
[44] Veerman J, Saakes M, Metz SJ, Harmsen GJ. Reverse electrodialysis: A validated process model for design and optimization. Chem Eng J 2011;166(1):256–68.
[45] Long R, Li B, Liu Z, Liu W. Reverse electrodialysis: Modelling and performance analysis based on multi-objective optimization. Energy. 2018;151:1–10.
[46] Long R, Li B, Liu Z, Liu W. Performance analysis of reverse electrodialysis stacks: Channel geometry and flow rate optimization. Energy 2018;158:427–36.
[47] Veerman J, de Jong RM, Saakes M, Metz SJ, Harmsen GJ. Reverse electrodialysis: Comparison of six commercial membrane pairs on the thermodynamic efficiency and power density. J Membr Sci 2009;343(1):7–15.
[48] Alsaman AS, Askalany AA, Harby K, Ahmed MS. Performance evaluation of a solar-driven adsorption desalination-cooling system. Energy 2017;128:196–207.
[49] Amirfakhraei A, Zarei T, Khorshidi J. Performance improvement of adsorption desalination system by applying mass and heat recovery processes. Therm Sci Eng Prog 2020;18:100516.
[50] Chua HT, Ng KC, Malek A, Kashiwagi T, Akisawa A, Saha BB. Modeling the performance of two-bed, sillica gel-water adsorption chillers. Int J Refrig 1999;22(3):194–204.